



**HAL**  
open science

# Poroelastic and Poroplastic Modeling of Hydraulic Fracturing in Brittle and Ductile Formations

Hanyi Wang, Matteo Marongiu-Porcu, Michael J. Economides

► **To cite this version:**

Hanyi Wang, Matteo Marongiu-Porcu, Michael J. Economides. Poroelastic and Poroplastic Modeling of Hydraulic Fracturing in Brittle and Ductile Formations. *SPE Production & Operations*, 2016, 31 (01), pp.47 - 59. 10.2118/168600-PA . hal-01626427

**HAL Id: hal-01626427**

**<https://hal.science/hal-01626427v1>**

Submitted on 30 Oct 2017

**HAL** is a multi-disciplinary open access archive for the deposit and dissemination of scientific research documents, whether they are published or not. The documents may come from teaching and research institutions in France or abroad, or from public or private research centers.

L'archive ouverte pluridisciplinaire **HAL**, est destinée au dépôt et à la diffusion de documents scientifiques de niveau recherche, publiés ou non, émanant des établissements d'enseignement et de recherche français ou étrangers, des laboratoires publics ou privés.

# Poroelastic and Poroplastic Modeling of Hydraulic Fracturing in Brittle and Ductile Formations\*

HanYi Wang, The University of Texas at Austin, Matteo Marongiu-Porcu, Schlumberger, Michael J. Economides, University of Houston

## Summary

The prevailing approach for hydraulic fracture modeling relies on Linear Elastic Fracture Mechanics (LEFM). Generally, LEFM that uses stress intensity factor at the fracture tip, gives reasonable predictions for hard rock hydraulic fracturing processes, but often fails to give accurate predictions of fracture geometry and propagation pressure in formations that can undergo plastic failures, such as poorly consolidated/unconsolidated sands and ductile shales. The reasons are that the fracture process zone ahead of the crack tip, elasto-plastic material behavior and strong coupling between flow and stress cannot be neglected in these formations. Recent laboratory testing has revealed that in many cases fracture propagation conditions cannot be described by traditional LEFM models. Rather, fractures develop in cohesive zones. In this study, we developed a fully coupled poro-elasto-plastic hydraulic fracturing model using cohesive zone method, which is not only able to model fracture initiation and growth considering process zone effects, but can also capture the effects of plastic deformation in the bulk formation. The impact of the formation plastic properties on the fracture process is investigated, and the results are compared with existing models. In addition, the effects of different parameters on fracture propagation in ductile formations are also investigated through parametric study. The results indicate that plastic and highly deforming formations exhibit higher breakdown and propagation pressure. The more plastic the formation (lower cohesion strength), the higher is the net pressure required to propagate the fracture due to increased plastic deformation. Also, lower cohesion strength leads to shorter and wider fracture geometry. The effect of formation plasticity on a hydraulic fracture is mostly controlled by initial stress contrast, cohesion strength of formation rock and pore pressure. We also found that altering the effective fracture toughness can only partially mimic the consequences of increased toughness ahead of the fracture tip in ductile formations, but it fails to capture the effect of plastic deformation within the whole affected area, which can lead to underestimating the fracture width and overestimating the fracture length. For a more accurate modeling of fracturing in ductile formations, the whole plastic deformation region induced by the propagating fracture should be considered, especially when shear failure areas are large.

## Introduction

Hydraulic fracturing has been widely used as a common practice to enhance the recovery of hydrocarbons from low to very low permeability reservoirs, as well as prevent sand production in high permeability reservoirs (Economides and Nolte 2000). Development of theoretical models of hydraulic fracturing started several decades ago, and provided a basis for hydraulic fracturing design, optimization and diagnostics. As a stimulation tool, the problem of hydraulic fracturing is in essence one of predicting the shape of the fracture as a function of time, given the fluid pressure at the wellbore or the flow rate into the fracture. Even today, modeling fluid-driven fracture propagation is still a challenging problem. The mathematical formulation of the problem is represented by a set of nonlinear integro-differential equations. Also, the problem has a moving boundary where the governing equations degenerate and become singular. The complexity of the problem often restricts researchers to consider only simple fracture geometries. An assumption commonly made is that the rock is linearly elastic and the loss of fluid into the rock is evaluated using a one-dimensional diffusion equation. The mechanics of fracture opening and fluid loss are considered independent and their interaction is not considered, such as the KGD model (Geertsma and De Klerk 1969; Khristianovich and Zheltov 1955) and PKN model (Nordgren 1972; Perkins and Kern 1961). In order to include the effect of fluid diffusion in porous media, many numerical models have been proposed based on the theory of poroelasticity (Adachi and Detournay 2008; Carrier and Granet 2013; Detournay and Garagash 2003). Although classic hydraulic fracturing simulators based on LEFM are convenient to use and can give reasonable predictions for brittle formations, they often fail to predict fracturing pressure and geometry with enough certainty in formations that can undergo plastic failures, such as poorly consolidated/unconsolidated sands and ductile shales.

By the proposition of Orowan (1955) and Irwin (1957), the medium around a crack tip can be divided into two regions, defined as "Process Zone" and "Universal Singularity", as illustrated in **Fig.1**. All microscopic details (complex processes of bond breaking and non-elastic behavior in front of the crack tip) are lumped together and hidden in the Process Zone. The assumptions behind the LEFM are that the material is linear elastic in the entire region right up to the point of crack tip, and the Process Zone is negligibly small compared to the macroscopic dimensions of the crack, so the stress and strain fields in the region of Universal Singularity (stress surrounding the crack tip develops a square root singularity) can have a singular form which is given by the so-called Stress Intensity Factors.

\*:1) This is uncorrected proof

2) Citation Export: Wang, H., Marongiu-Porcu, M., and Economides, M. J. 2016. Poroelastic and Poroplastic Modeling of Hydraulic Fracturing in Brittle and Ductile Formations, Journal of SPE Production & Operations, 31(01): 47–59.  
<http://dx.doi.org/10.2118/168600-PA>

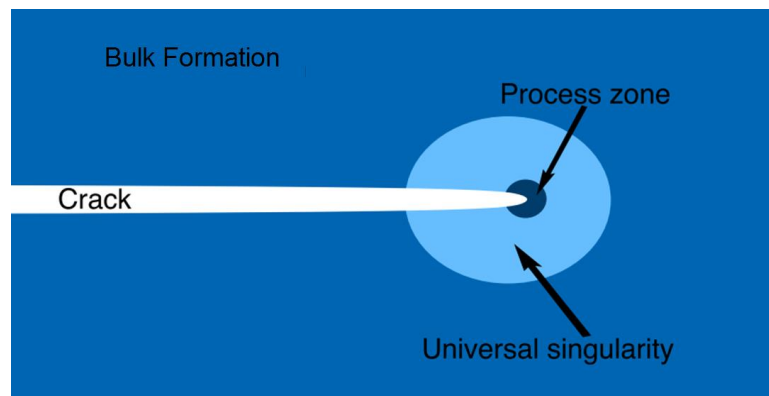


Fig. 1—Regions around the tip of a propagating crack

Numerous laboratory studies have shown that deformation of weakly cemented sands and ductile shales can even occur through elastic-visco-plastic constitutive behavior, and the deformations of these types of rocks cannot be predicted by linear elasticity (Sone and Zoback 2011). Ductile rocks often exhibit soft behavior (low Young's modulus) and according to the theory of LEFM, the lower the Young's modulus, the lower the propagating pressure. However, on the contrary, many field study and surveys found that the net pressures observed in ductile formations are much higher than that predicted by LEFM, especially in unconsolidated sands, and these observations have triggered a series of dedicated studies which looked into the importance of the plastic deformation in hydraulic fracturing (Germanovich et al. 1998; Papanastasiou 1997; Papanastasiou 1999; Van Dam et al. 2002). The disparities between field observations and the results predicted by LEFM indicate that the complex phenomena in the process zone beyond the fracture tip, elasto-plastic rock behavior and strong coupling between flow and stress cannot be neglected in these ductile formations.

Besides the commonly known poorly consolidated/unconsolidated sands, the fact that shale rocks can also exhibit in-elastic behavior has been largely ignored in both industry and academia. Not all shales are as brittle as the Barnett shale; depending on mineral compositions (such as clay, carbonates, quartz, etc.), many shales can exhibit a pronounced ductile behavior, such as the Eagle Ford and the Haynesville Shale. The ductile nature of these shale plays poses a challenge in hydraulic fracturing design and execution. Field studies indicate that it is more difficult to initiate a hydraulic fracture in ductile Haynesville shales (Parker et al. 2009), and the production from hybrid fracturing treatments (creating highly conductive primary fractures) wells outperforms the water-frac (creating large fracture surface area) wells in the Eagle Ford shale (Stegent et al. 2010); this demonstrates that creating a high-conductivity fracture may be more critical to long-term production than creating large surface area in ductile shales. Such trends can be explained by the fact that in clay-rich ductile shale, the level of complexity of the induced hydraulic fracture geometry is relatively low, dominant "bi-wing" fractures are more likely to occur and unpropped fractures will most likely not be conductive after initial production. Thus, being able to predict fracture geometry and fracturing pressure with enough confidence is not only important in poorly consolidated/unconsolidated sands, but also crucial in ductile shales, because of the long term production hinges on the portion of the primary fracture that can be propped with enough size and concentration of proppants. A completely different scenario (beyond the domain of interest of this study) opens up when a hydraulic fracture propagates in naturally fractured brittle formations, where the interaction with pre-existing natural fractures becomes the dominant phenomenon (Weng 2014).

In examining the plentiful literature concerning fracture mechanics, the cohesive zone modeling has been adopted by many authors to model fracture initiation and propagation by considering the effects of in-elastic behavior in front the fracture tip. The cohesive zone is a region ahead of the crack tip that is characterized by micro-cracking along the crack path. The main fracture is formed by interconnection of these micro cracks due to damage evolution. The physical meaningless tip singularity predicted by LEFM can be resolved with the idea of cohesive zone model (Mokryakov 2011). The conception of cohesive zone was first introduced by Barenblatt (1959; 1962) to investigate fracture propagation in perfectly brittle materials. In order to investigate fracture damage behavior in ductile materials with small scale of plasticity, a fracture process zone was proposed by Dugdale (1960), that adopt a critical opening condition as a fracture criterion. Mathematically, the Dugdale (1960) model is similar to the Barenblatt model with the exception that different conditions (the condition of constant cohesive zone length and the condition of maximal cohesive zone opening) were applied to the cohesive zone parameters. Because cohesive properties in the cohesive zone are material parameters that do not depend on fracture dimensions and loading. The classical Griffith's brittle elastic fracture model (1921) is a limited case of Barenblatt's model: if the cohesive zone length tends to zero (with respective increase of the cohesive stress) then, in the limit, the stress-strain state corresponding to the classic square root asymptotes will be obtained.

In recent works of adapting cohesive zone method for modeling of hydraulic fracturing, Dean and Schmidt (2009) proposed a fully coupled geo-mechanical reservoir simulator that incorporates two different fracture propagation criteria: a conventional LEFM criterion based on stress intensity factor and a cohesive strength criterion based on energy release rate, within the

cohesive zone in front of propagating hydraulic fracture tip. Chen et al. (2009) established a model based on the existing pore pressure cohesive finite elements to investigate the propagation of a penny-shaped hydraulic fracture in an infinite elastic medium. The finite element results match well with the analytical solutions where the fracture process is dominated by rock fracture toughness. Mokryakov (2011) proposed an analytical solution for hydraulic fracture with Barenblatt's cohesive zone based on the KGD model by assuming impermeable elastic rock without considering leak-off. It shows that the derived solutions from cohesive zone model can fit the pressure log much more accurately than LEFM for the case of fracturing ductile formations. Sarris and Papanastasiou (2012) developed a poroelastic cohesive zone model and investigated the effects of permeability, injection rate and formation compressibility on fracture geometry, it is concluded that higher pressures are needed to extend a fracture in a poroelastic medium than in an elastic medium. Yao (2012) developed a 3D cohesive zone model to predict fracture propagation in brittle and ductile rocks and the effective fracture toughness method was proposed to include the process zone effect on fracturing in ductile rock. The results show that with the increase of effective fracture toughness, the cohesive zone model gives predictions that are more conservative on fracture length as compared with pseudo 3D and PKN models.

Even though all these models are able to account for in-elastic behavior beyond the fracture tip by lumping all the effects into the cohesive zone, they do not consider plastic deformation in the formation bulk. In reality, depending on the in-situ stresses and rock properties, the plastic deformation can occur at a certain distance from the fracture tip, without limiting itself to the very close vicinity of the fracture tip. In this study, we developed a hydraulic fracture model for both poroelastic and poroplastic formations based on the cohesive zone method, where the effects of plastic deformation in the whole simulated region are included. The physical process involves full coupling of the fluid leak-off from fracture surface and diffusion into the porous media, the rock deformation and the fracture propagation. The model is then solved by finite element method. We investigated how the plastic failures and fluid/rock interactions can impact the fracture geometry, breakdown and propagation pressure in ductile formations and the results are compared with that in brittle formations. Additional content and further discussions on fracture reorientation, multiple fracturing and producing well interference in both brittle and ductile reservoir rocks are presented in companionate articles (Wang 2015a; 2015b)

## Mathematical Model

Following fracture initiation, further fluid injection results in fracture propagation. the geometry of the created fracture can be approximated by taking into account the mechanical properties of the rock, the properties of the fracturing fluid, the conditions with which the fluid is injected (rate, pressure), and the stresses and stress distribution in the porous medium. In describing fracture propagation, which is a particularly complex phenomenon, two sets of laws are required: (i) Fundamental principles such as the laws of conservation of momentum, mass and energy, and (ii) criteria for propagation that include interactions of rock, fluid and energy distribution.

## General Equations

A wide variety of fluids have been used for fracturing including water, aqueous solutions of polymers with or without crosslinkers, gelled oils, viscoelastic surfactant solutions, foams, and emulsions. Most hydraulic fracturing fluids for high permeability formations exhibit power law rheological behavior and temperature-related properties, while for low permeability unconventional formations, water is commonly used as hydraulic fracturing fluid. In order to avoid additional complexity added by fluid behavior, incompressible and Newtonian fluid is assumed in this study. The continuity equation which imposes the conservation of mass in one dimensional flow is (Boone and Ingraffea 1990)

$$\frac{dq_f}{dx} - \frac{dw}{dt} + q_l = 0, \dots \dots \dots (1)$$

where  $q_f$  is the local flow rate per unit height along the fracture in direction  $x$ ,  $q_l$  is the local fluid loss in rock formation per unit fracture surface area and  $w$  is the crack opening. Eq. 1, the local flow rate  $q_f$  can be determined by taking fluid leak-off into consideration. Carter's Leak-off model is used in this study to describe the leak-off phenomena (Howard and Fast 1970):

$$v_L = \frac{C_L}{\sqrt{t}}, \dots \dots \dots (2)$$

$$\frac{V_L}{A_L} = 2C_L\sqrt{t} + S_p, \dots \dots \dots (3)$$

where  $v_L$  is leak-off velocity,  $C_L$  is leak-off coefficient,  $t$  is the time elapsed since the start of the leakoff process,  $V_L$  is the cumulative fluid volume that passes through the surface  $A_L$  during the time period from time zero to time  $t$ , the integration constant  $S_p$  is called spurt loss, which represents a sudden fluid loss into the formation when new fracture surface area are created and a stable leakoff status has not been established yet within the newly create fracture surface area. The two coefficients  $C_L$  and  $S_p$ , can be determined from laboratory tests or, preferably, from the evaluation of Fracture Calibration

Tests (FCT), which is also often referred to as MiniFrac, Mini-Fall-off (MFO) and Diagnostic Fracture Injection Test (DFIT) in literature. Nottle (1986), Valkó and Economides (1999) and Marongiu-Porcu et al. (2014) presented vast theoretical modeling and field example analyses on this specific subject. For high permeability formations, spurt loss can contribute to the majority of the fluid leakoff volume even with the addition of leakoff prevention additives. For low permeability formations, spurt loss is negligible unless the fissure system is considered, if present. Setting  $A_L$  to be the unit surface area, and discretizing Eq. 3 with respect to time, the difference of cumulative leakoff volume  $V_L$  between each time intervals can be calculated. When the discretized time intervals are small enough, the changes of cumulative leakoff volume  $V_L$  divided by time interval are approximate to the leakoff rate per unit surface area,  $q_L$ , within that specific time interval. For a flow between parallel plates, the conservation equation of momentum balance can be used to relate the pressure gradient to the fracture width for a Newtonian fluid of viscosity  $\mu$  (Boone and Ingraffea 1990):

$$q_f = uw = -\frac{w^3 dp}{12\mu dx}, \dots \dots \dots (4)$$

where  $p$  is the fluid pressure inside the fracture and  $u$  is the average fluid velocity over the cross-section of fracture. Pressure drop along the fracture can be determined by Eq. 4 with local flow rate and local fracture width. Darcy's Law is used to describe fluid diffusion in the isotropic, porous media:

$$q_m = -\frac{k}{\mu} \nabla p, \dots \dots \dots (5)$$

where  $\nabla p$  is the formation pressure gradient vector,  $q_m$  is the fluid flux velocity vector in the porous media,  $k$  is formation permeability tensor. When the porous medium considered is isotropic, the permeability tensor will appear in its diagonal form, with equal valued elements on the diagonal. Biot's poroelastic theory (1941) is used to couple rock deformation and pore pressure. Together with fluid mass conservation, the whole system of fluid-rock deformation can be solved with appropriate initial and boundary conditions.

### Fracture Initiation and Propagation

There is a number of fracture propagation criteria have been proposed by previous studies, which is usually described by either a stress condition or an energy condition. The propagation criterion introduced within the context of LEFM assumes that the process zone is negligible compared to the fracture size, and a fracture can propagate only if the stress intensity factor exceeds the material toughness. However, fracture propagation in ductile formations can induce a significant plastic deformation around the fracture due to shear failure, which put the adequacy of such assumptions into questioning. The cohesive zone model that takes the process zone into consideration is able to capture non-linear fracture mechanics behavior based on energy condition, and a fracture will propagate when the energy release rate in the process zone reaches a critical value. The cohesive method proposed by Barenblatt (1959; 1962) assumed that the cohesive zone length and the cohesive stress distribution are material parameters that do not depend on fracture dimensions and loading. The classical Griffith's (1921) brittle elastic fracture model is a limited case of Barenblatt's model: if the cohesive zone length tends to zero (with respective increase of the cohesive stress) then, in the limit, the stress-strain state corresponding to the classic square root asymptotes will be obtained. In essence, cohesive zone is way of representing the process in front of fracture tip mathematically.

The constitutive behavior of the cohesive zone is defined by the traction-separation relation, which includes initial loading, initiation of damage, and the propagation of damage that leading to eventual failure at the bonded surface. The behavior of the interface prior to initiation of damage is often described as linear elastic in terms of a penalty stiffness that degrades under tensile and/or shear loading but is unaffected by pure compression. Laboratory experiments can be used to derive these relations by investigating post-peak behavior with principle/shear stress and axial/shear strain data. A cohesive potential function  $G$  is defined so that the traction is given by

$$T = \frac{\partial G}{\partial \delta}, \dots \dots \dots (6)$$

where  $T$  is traction force and  $\delta$  is the displacement across a pair of cohesive surfaces. For Mode-I fracture (induced by forces that are perpendicular to the crack), the traction force  $T$  can be interpreted as a tensile stress in front of fracture tip. Based on different types of materials, different forms of traction-separation relations in cohesive zones can be adopted to simulate the dynamic fracture process.

Tomar et al. (2004) proposed a bilinear cohesive law, as shown in **Fig. 2**. It assumes that the material exhibit linear elastic behavior before the traction reaches the tensile strength  $T_{Max}$  or the separation of cohesive surfaces exceeds the displacement of damage initiation,  $\delta_0$ . Beyond  $\delta_0$ , the traction reduces linearly to zero up to the displacement of complete failure  $\delta_f$  (linear softening), and any unloading takes place irreversibly. For mode-I plane strain fracture, the critical fracture energy  $G_f^c$  equals

the area under the traction-separation curve, which can be related to the rock fracture toughness  $K_{IC}$  by (Kanninen and Popelar 1985):

$$G_I^c = \frac{K_{IC}^2}{E}(1 - \nu^2), \dots \dots \dots (7)$$

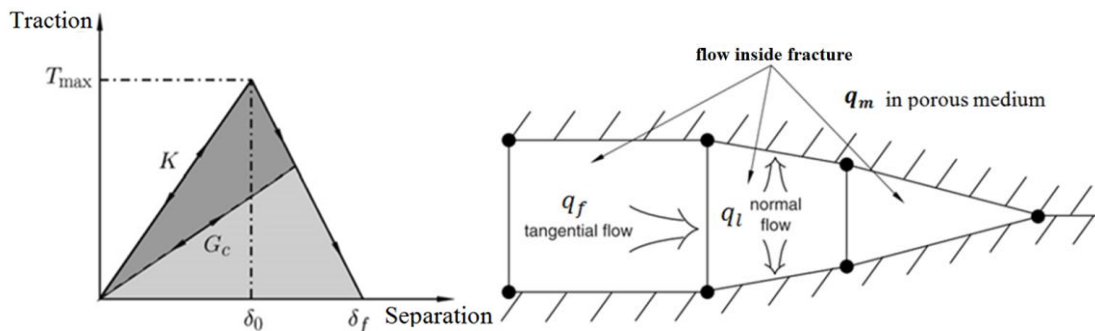


Fig. 2–Traction-Separation law and fluid inside cohesive surface

where  $E$  is Young’s modulus of formation and  $\nu$  is Poisson’s ratio. Alternative, the critical fracture energy can be determined by laboratory experiment. For bilinear traction-separation law, displacement of complete failure  $\delta_f$  can be determined by:

$$\delta_f = \frac{2G_I^c}{T_{Max}} = \frac{2K_{IC}^2(1 - \nu^2)}{ET_{Max}}. \dots \dots \dots (8)$$

The stress-displacement relation in the initial part of the loading curve corresponds to linear elastic deformation as follows:

$$\sigma = \frac{\delta T_{Max}}{\delta_0} = \delta K_n, \dots \dots \dots (9)$$

where  $K_n$  is the stiffness of the stress-displacement relation in the loading regime and is assumed to be equivalent to the stiffness of formation according to the following equation:

$$\sigma = \delta K_n = \frac{E\delta}{d}, \dots \dots \dots (10)$$

where  $d$  is the initial thickness of cohesive surfaces and the post-peak linear softening regime is given by the following:

$$\sigma = T_{Max} \left[ 1 - \frac{(\delta - \delta_0)}{(\delta_f - \delta_0)} \right], \dots \dots \dots (11)$$

Typically, conventional hydraulic fracture models based on LEFM employ Mode-I based fracture criteria that only consider tensile failure mechanism in fracture propagation. However, shear failure may play an important role in ductile formations under certain loading conditions. The traction-separation law presented above for Mode-I based fracture criteria can be easily extended to mixed-mode fracture criteria. For an isotropic formation, the traction-separation responses in different modes are assumed to be the same in this study, as shown in **Fig. 3**. where  $t_n, t_s, t_t$  refer to the normal, the first, and the second shear stress components on the cohesive interface; and  $t_n^0, t_s^0, t_t^0$  represent the tensile strength of the rock material when the deformation is purely perpendicular to the interface and the shear strength of rock material in the first and the second shear direction;  $\delta_n^0, \delta_s^0, \delta_t^0$  correspond to the displacements of initial damage in the normal, the first, and the second shear stress direction and  $\delta_n^f, \delta_s^f, \delta_t^f$  are the displacements of complete failure in these three directions.

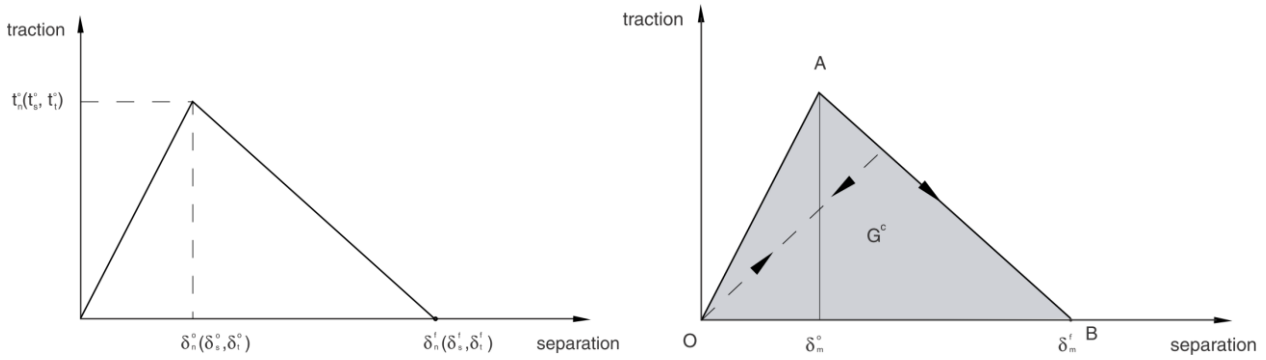


Fig. 3–Traction-Separation law for mix-modes

Damage is assumed to initiate when one of the stress components reaches the value of maximum strength of rock material, which can be represented by a quadratic law

$$\left\{ \frac{\langle t_n \rangle}{t_n^0} \right\}^2 + \left\{ \frac{t_s}{t_s^0} \right\}^2 + \left\{ \frac{t_t}{t_t^0} \right\}^2 = 1. \quad \dots\dots\dots (12)$$

The symbol  $\langle \rangle$  used in the above equation represents the Macaulay bracket with the usual interpretation. The Macaulay brackets are used to signify that a pure compressive deformation or stress state does not initiate damage. The stress components of the traction-separation model are affected by the damage according to

$$\mathbf{t} = \begin{cases} (1 - D)\bar{\mathbf{t}} & \text{damage initiated} \\ \bar{\mathbf{t}} & \text{no damage occurs} \end{cases}, \quad \dots\dots\dots (13)$$

where  $\mathbf{t}$  are stress components,  $\bar{\mathbf{t}}$  are the stress components predicted by the elastic traction-separation behavior for the current strains without damage.  $D$  is a scalar damage variable, which has an initial value of 0 and monotonically increases to 1 as damage developing, represents the overall damage that comes from the combined effects of different traction-separation modes in the rock material. For linear softening as shown in Fig. 3, the evolution of the damage variable,  $D$ , reduces to (Turon et al. 2006)

$$D = \frac{\delta_m^f (\delta_m^{max} - \delta_m^0)}{\delta_m^{max} (\delta_m^f - \delta_m^0)}, \quad \dots\dots\dots (14)$$

where  $\delta_m$  is effective displacement, defined as

$$\delta_m = \sqrt{\langle \delta_n \rangle^2 + \delta_s^2 + \delta_t^2}. \quad \dots\dots\dots (15)$$

The mode mix of the deformation fields in the cohesive zone quantify the relative proportions of normal and shear deformation. The the Benzeggagh–Kenane fracture criterion (Benzeggagh and Kenane 1996) is implemented in this model to determine the mixed-mode damage evolution during fracture propagation. This criterion is suitable for situation when the critical fracture energy of rock material along the first and the second shear directions are similar. The combined energy dissipated due to failure,  $G^c$ , is defined as

$$G^c = G_I^c + (G_{II}^c - G_I^c) \left( \frac{G_{shear}}{G_{total}} \right)^\eta, \quad \dots\dots\dots (16)$$

where  $G_{shear} = G_{II}^c + G_{III}^c$ ,  $G_{total} = G_{shear} + G_I^c$ . And  $G_I^c, G_{II}^c, G_{III}^c$  are the work done by the tractions and their conjugate relative displacements in the normal, first, and second shear directions. For isotropic failure assumed in this study where  $G_{II}^c = G_I^c$ , the cohesive response is insensitive to parameter  $\eta$ , and the fracture will propagate when the energy release rate reaches  $G_I^c$ .

### Simulation Model

When fluid is pumped into the reservoir at a sufficiently high pressure, the reservoir rock will break down and open. Continued pumping of the fluid at this pressure will propagate the induced crack into the reservoir. In this model, a pre-defined surface made up of elements that support the cohesive zone traction-opening calculation is embedded in the rock and the hydraulic fracture grows along this surface. This typical cohesive zone model is illustrated in Fig. 4. The fracture process zone

(unbroken cohesive zone) is defined within the separating surfaces where the surface tractions are nonzero (Traction-Separation law is still valid). The fracture is fully filled with fluid in the broken cohesive zone where no traction from rock fracture exists but fluid pressure is acting on the open fracture surfaces. When the energy release rate reaches the critical value  $G^c$  in front of the propagating fracture tip (unbroken cohesive zone), the associated cohesive element will be completely damaged and fluid filled fracture will propagate.

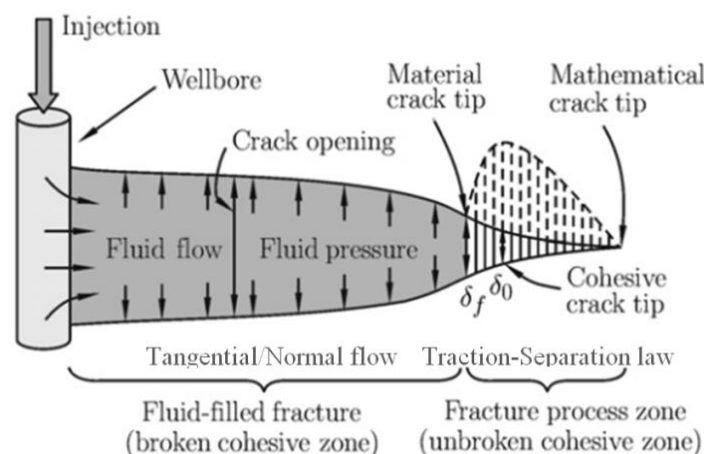


Fig. 4—Cohesive zone embedded along fracture path (Modified from Chen et al., 2009)

In this study, a two dimensional plane strain fluid-driven fracture in porous rock is simulated and a close view of this model is shown in Fig. 5. (The actual simulation domain is much larger to reduce the influence of boundary effects). The initial separation along the fracture path is set zero that represents intact formation and the cohesive elements at the perforation points are defined as initially open to allow entry of the fluid at the perforation tunnel(s), so that the initial flow and fracture growth are possible. The whole area is saturated with reservoir fluid and incompressible Newtonian fluid is injected at a constant rate at the perforation. Grid size along the fracture path is 0.2 m and all the displacements of outer boundaries are fixed. It should be emphasized that the CZM used in this article is implemented by an artificially pre-defined path of cohesive element that embedded along element edges. The cohesive element glues 2 conjugated cohesive surfaces of the reservoir pressure–displacement element. Under different local stress conditions, the behavior of these cohesive surfaces are governed by the traction-separation laws in normal or shear directions, as depicted by Fig2 (left side) and Fig3. When the cohesive element is completely damaged, the bounded two cohesive surfaces detached and hydraulic fracture propagates.

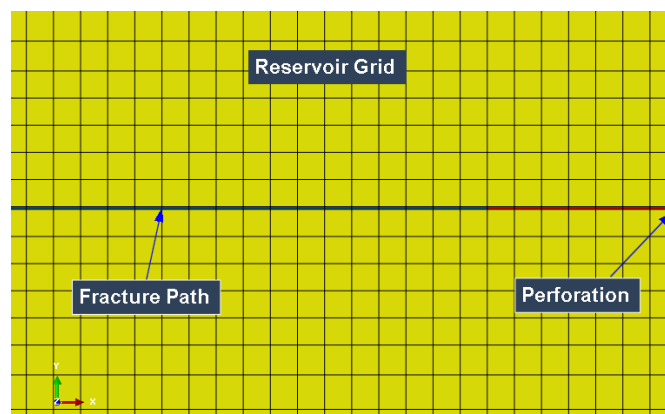


Fig. 5—Initial reservoir and fracture grid around fracture path

The inelastic rock material behavior follows the Mohr-Coulomb flow theory of plasticity for a cohesive frictional dilatant material. Associative behavior with constant dilatation angle is considered. These assumptions are justified by the presence of high confining stresses prior to crack propagation and to a decrease in the initial in-situ mean pressure near the crack tip during propagation. The Mohr-Coulomb criterion assumes that yield occurs when the shear stress on any plane in a material reaches the same value as shear strength, which is defined as:

$$\tau_f = c + \sigma_n \tan \phi, \dots \dots \dots (17)$$



where  $\tau_f$  is shear strength,  $c$  is cohesion strength,  $\sigma_n$  is the stress normal to a specific plane,  $\varphi$  is the friction angle. And the ratio of rate of plastic volumetric strain to the rate of plastic shear distortion is controlled by dilation angle (Vermeer and De Borst 1984). Ductile shales and sandstones can have cohesion strengths that ranges between 3MPa and 8MPa, while the cohesion strength of poorly consolidated sands and shales with planes of weaknesses is normally below 3MPa (Afrouz 1992). Nassir (2013) incorporated elasto-plastic behavior in modeling shear fracturing in shale reservoirs; this work shows that the effective rock cohesion in naturally fractured shale formations should be less than 1 MPa to justify a reasonable size of stimulated reservoir volume (SRV) induced by shear failure observed in the field. **Table 1** shows all the input parameters for the synthetic base case simulation in this study, which would fit in the context of a ductile shale formation that contains micro-fractures.

Input Parameters	Value
Young's modulus	20 GPa
Poisson's ratio	0.25
Fluid viscosity	1 cp
Tensile strength	2 MPa
Formation effective permeability	1 md
Injection rate per unit thickness	0.0005 (m <sup>3</sup> /s/m)
Specific weight of fluid	9.8 kN/m <sup>3</sup>
Initial pore pressure	20 MPa
Maximum horizontal stress	42 MPa
Minimum horizontal stress	37 MPa
Vertical stress	65 MPa
Fracture toughness	1 MPa√m
Carter's leakoff coefficient	2.00E-06 m/√s
Spurt loss coefficient	2.5E-04 m
Porosity	0.1
Friction angle	27°
Dilation angle	8°
Cohesion strength	4 MPa

**Table 1– Input parameters for base case simulation**

The numerical solution procedure is schematically illustrated in **Fig. 6**. The coupled system of non-linear equations is solved numerically by Newton-Raphson method, which requires evaluating Jacobian matrix, start from initial guess values to approximate to the solution through successive iterations. All the variables in the system are updated at the end of each time increment and input as initial values at the start of the next increment. The program for numerical calculations was developed using FORTRAN and finite element package ABAQUS.

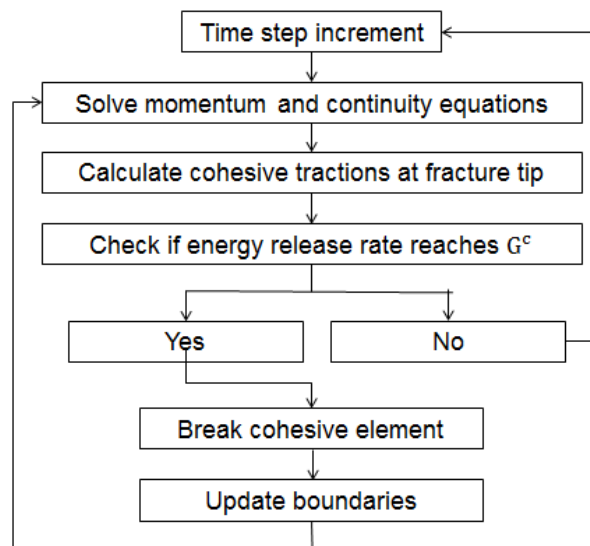


**Fig. 6–Solution flow diagram for fracture propagation procedure.**

In the following part, we'll compare the simulation results from our poro-elasto-plastic model with other existing models from literature to reveal how the fracture geometry, the net pressure and the fluid efficiency can be impacted by plastic deformations due to shear failure, then we carry out a set of parametric studies to determine which parameters mostly control the influence of plasticity on fracture propagation in ductile formations.

## Results and Analysis

In this section we present our simulation results to demonstrate the importance of plasticity in modeling hydraulic fracturing in ductile formations. Our simulation results are compared with two other cohesive zone based hydraulic fracture models, which are the poroelastic model (Sarris and Papanastasiou 2012) and the poroelastic model with effective toughness (Yao 2012).

The idea of using effective toughness is to modify the poroelastic model, by lumping all plastic deformation effects into an increased toughness beyond the fracture tip (Papanastasiou 1999). In principle, the effective toughness can be determined either by investigating experimentally the formation rock softening behavior, or by matching the predicted net pressure to the actual net pressure data from a FCT. In this study, the effective toughness is determined by matching the poroelastic model calculated net pressure to the one predicted by our fully coupled poro-elasto-plastic model. The final adjusted effective toughness for the poroelastic model is 3 times larger ( $3 \text{ MPa}\sqrt{m}$ ) than the original toughness ( $1 \text{ MPa}\sqrt{m}$ ) declared in Table 1.

**Fig. 7** shows the net pressure predicted by three different models investigated in this study. The predicted net pressure from poroelastic model with increased effective toughness matches the net pressure from poro-elasto-plastic model significantly well, while the predicted net pressure from poroelastic model keeps itself at much lower values throughout the entire simulated injection. This means that higher net pressure levels are actually needed to initiate and propagate hydraulic fractures in plastic formations. It should be mentioned that not only ductile formation itself can lead to difficulties in initiating hydraulic fracture (Parker et al. 2009), field study (Yuan et al. 2013) also indicates that perforations-associated damaged rock can behave like a plastic rubber buffering between the reservoir and fracture entry, which can lead to significant increase of formation breakdown pressure.

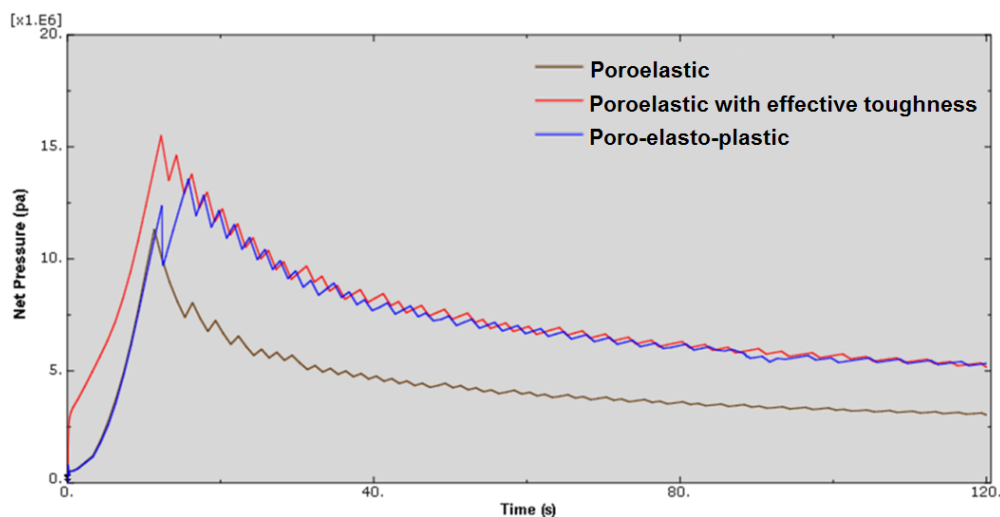


**Fig. 7—Net pressure prediction with different models**

However, as demonstrated in **Fig. 8**, the predicted fracture is wider in the poro-elasto-plastic model than in the poroelastic model with increased effective toughness, even though both models have the same matched net pressure. This is due to the fact that the effective toughness method considers uniquely the increased toughness within the very close vicinity of fracture tip due to rock plasticity, but it fails to capture the effects of plastic deformation that result from shear failure in the bulk formation induced by the instantaneous fracture propagation. So using CZM alone by increasing fracture toughness (i.e., increase critical fracture energy in the cohesive zone) is inadequate in modeling fracture propagation in ductile formations when the plastic damage is not constrained to the very close vicinity of fracture tip. Nevertheless, both models predict wider fracture widths than the poroelastic model, which does not consider formation plasticity at all.

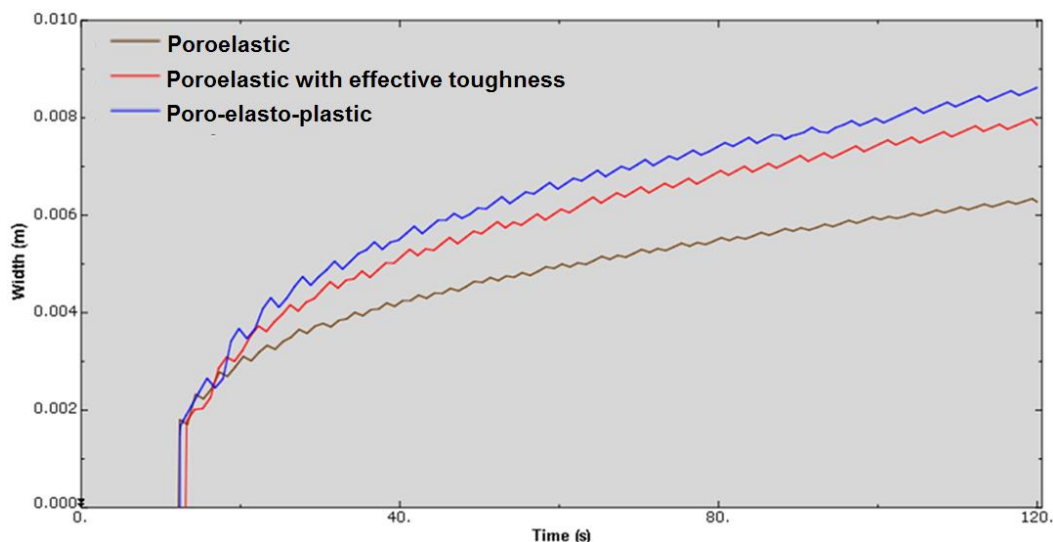


Fig.8—Maximum fracture width prediction with different models

**Table 2** shows the simulation results of 30 minutes of injection for the three different models, and we can observe that formation plasticity has a substantial impact on the fracture geometry after 30 minutes of injection. The predicted fracture length is reduced by nearly 38 % compared to the one predicted by the poroelastic model when plastic deformations are incorporated. In addition, the estimated fracture fluid efficiency is larger when plastic effects are considered because shorter fracture lengths lead to smaller leak-off surfaces. We can also observe that the use of the effective toughness can only partially mimic rock plasticity, even though it still provides wider and shorter fractures, but it fails to capture the effects of plastic deformations within the whole affected area. For a more accurate modeling of fracture propagation in ductile formations, the effects of the whole plastic deformation region should be included, especially when the shear failure area are large. Whenever this is not done, the fracture width is underestimated and the fracture length is overestimated, although good net pressure matches can be generated

	Poroelastic (Sarris and Papanastasiou 2012)	Poroelastic Using Effective Toughness (Yao 2012)	Poro-Elasto-Plastic
Fracture length (m)	80.6	58.8	50.2
Fracture width at wellbore (mm)	11.52	16.95	20.67
Fluid efficiency (%)	75.20	80.72	84.06

Table 2– Simulation results of 30-minute injection with different models

### Parametric Study

In this section we study the effects of different parameters on fracture propagation in ductile formations. The parameters include injection rate, leak-off coefficient, pore pressure, horizontal stress contrast and cohesion strength. In the parametric study only one parameter changes while all other input parameters are kept consistent with the base case.

### Injection Rate

The injection rate is increased to 5 times the base case. **Fig. 9** shows the impact of such injection rate on fracture geometry. It can be observed that wider fracture profiles can be obtained with faster propagation speed for larger injection rates, which in turn results in larger net pressures and wider plastic deformation. Because the fracture width does not increase significantly at a higher injection rate, the fracture propagation speed can be considered as approximately proportional to injection rate. At the end of the 2-minute injection, the fracture half-length with Qx5 injection rate is about 5 times longer than the base case.

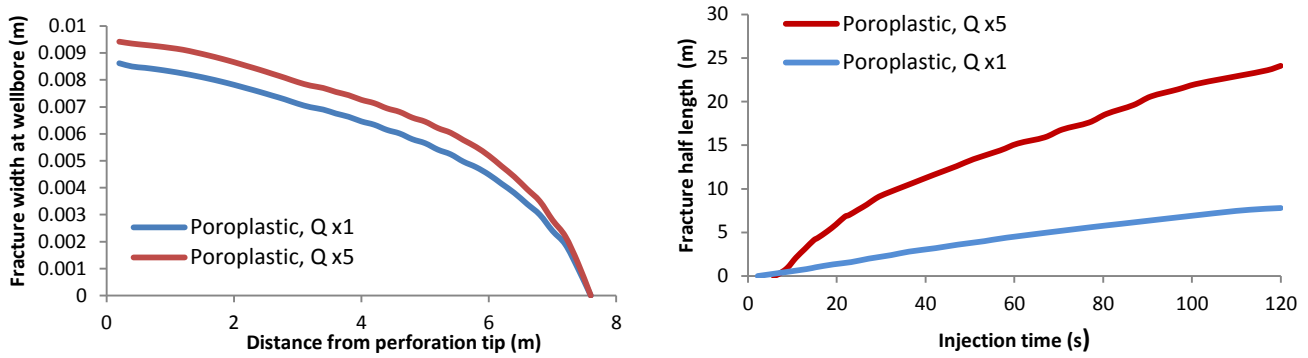


Fig. 9—Impact of injection rate on fracture geometry

### Leak-off Coefficient

Now we increase the leak-off coefficient 100 times and compare the results with the base case. From **Fig. 10**, we see that a larger leak-off rate leads to much shorter fracture length, because more fracturing fluid filtrates into the formation, but this appears to have a limited impact on the net pressure and the fracture width at the wellbore, as shown in **Fig. 11**. Slightly higher net pressure and smaller fracture width are obtained with higher leak-off rate due to poroelastic backstress (i.e., the induced additional confining stress around the fracture surface because of the increased local pore pressure). Even though the leak-off rate has been increased by 100 times, the reservoir permeability in this example is still large enough to allow the pore fluid to move freely and dissipate energy within the same timeframe as the fracture opening time, thus, the changes in pore pressure around the fracture and the poroelastic backstress induced by the extra leak off is relatively small. This shows that, ultimately, the leak-off coefficient has a larger impact on the fracturing fluid material balance (how much injection fluid is contributing to create fracture volume versus how much is leaking into the formation) than on the constitutive response of rock deformation, as long as the permeability is large enough that can prevent the buildup of local pore pressure.

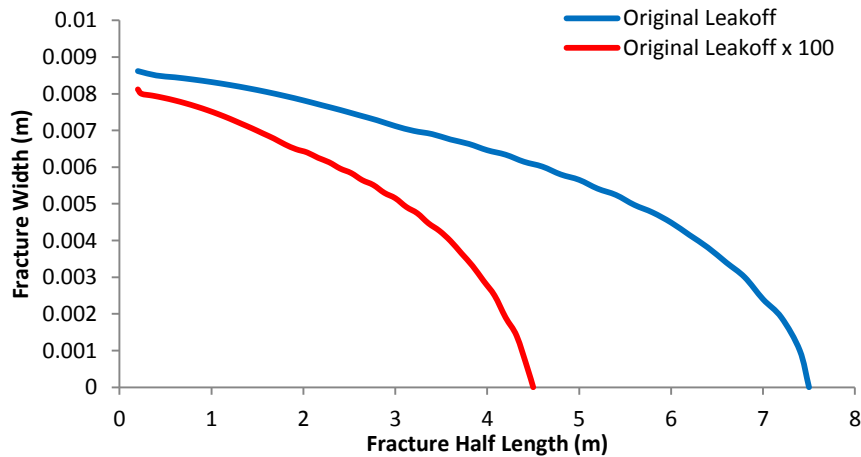


Fig. 10—Impact of leak-off coefficient on fracture length

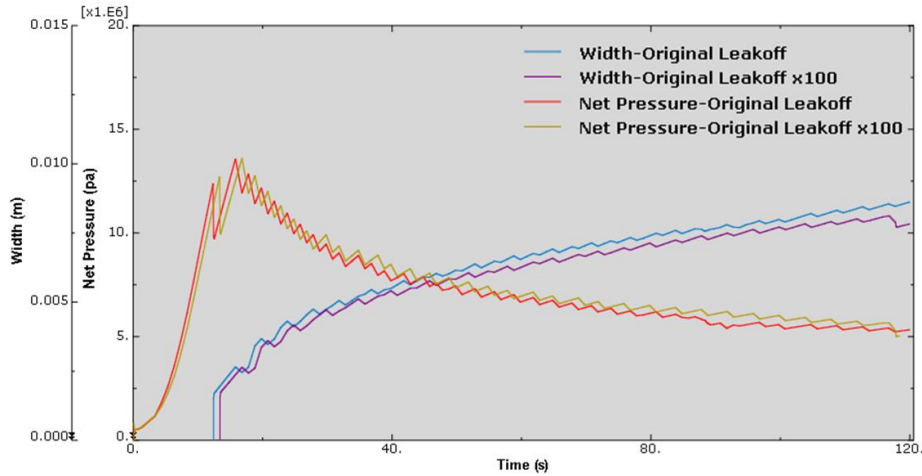


Fig. 11–Impact of leak-off coefficient on fracture net pressure and width

**Pore Pressure**

The formation pore pressure is increased from 10 MPa (base case) to 20 MPa, while maintaining the same far field stresses. **Fig. 12** shows the comparison between simulated net pressures with different pore pressures. The results clearly indicate that the lower the pore pressure, the lower the net pressure is needed to initiate and propagate the fracture. In turn **Fig. 13** shows that with higher formation pore pressure, the shear failure induced plastic strain increases (PEEQ denotes equivalent plastic strain), and the plastic deformation area becomes larger, which leads to a shorter and wider fracture geometry. The results also indicate that even a small amount plastic deformation (with PEEQ on the order of  $10^{-3}$ ) can make a significant difference in fracturing pressure and propagation geometry.

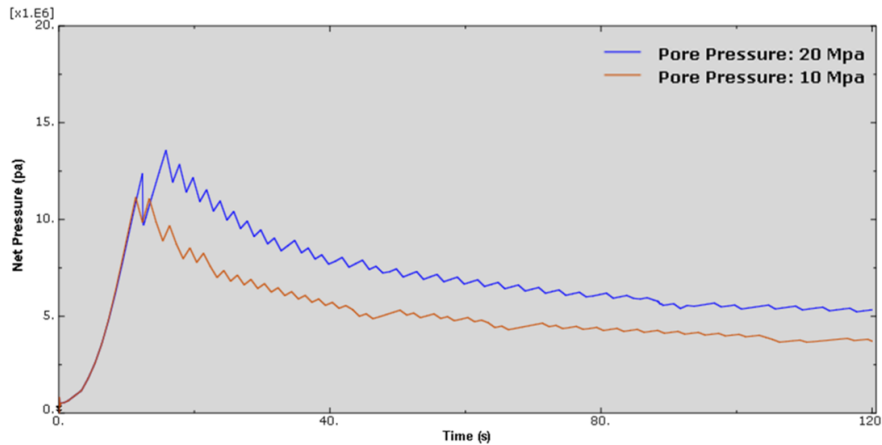


Fig. 12–Impact of pore pressure on net pressure

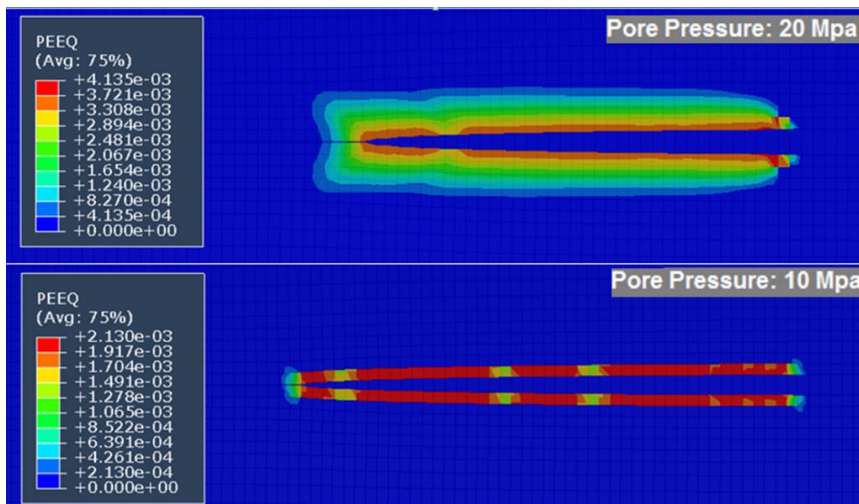
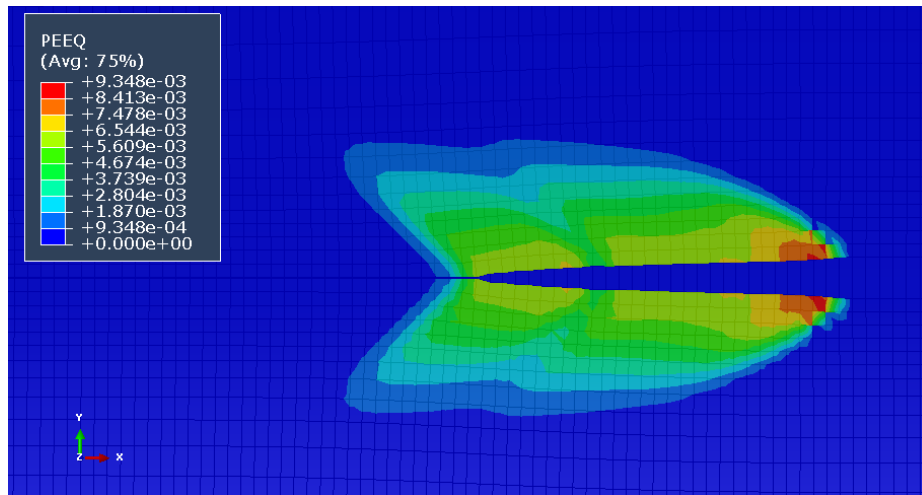


Fig. 13–Impact of pore pressure on plastic strain and fracture geometry

### Horizontal Stress Contrast

Trivially, the closer the initial reservoir stress conditions to the Mohr-Coulomb shear failure surface, more likely shear failure events will be triggered around the fracture during propagation. Here we investigate how the horizontal stress contrast impacts the plastic deformation by increasing such contrast from 1.1 (base case) to 2, and the results are shown in **Fig. 14**. Compared to the simulation results from base case as shown in Fig. 13 (lower illustration), it can be observed that a higher contrast between the initial minimum and maximum horizontal stresses leads to a shorter and wider fracture geometry with larger plastic deformation area. When the rock in-situ stress is far away from the shear failure envelop, additional stress induced by a hydraulic fracture may still not be large enough to cause shear failure at a certain distance from the fracture. However, when the rock is close to the shear failure envelop under initial condition, stress disturbance induced by the propagating fracture is able to push the rock into the failure envelop more easily, and a larger area around the propagating fracture can be impacted.



**Fig. 14**–Impact of higher horizontal stress contrast on plastic strain and fracture geometry

### Cohesion Strength

The cohesion strength reflects how well the rock grains are cemented, as well as rock resistance to shear failure. Reservoir porous rocks under differential stress can exhibit significant permanent deformation due to intergranular slip and rotation that overcomes the elastic deformation of the grains and grain contacts if the cohesion strength is low. In order to examine the impact of rock cohesion strength on hydraulic fracture propagation, we set the cohesion strength to be 2 MPa, 4 MPa and 6 MPa, to represent formations with relative low (unconsolidated sands or shale with weak planes), moderate (ductile shale with micro-fractures) and high cohesion strength (soft sandstone) in this study.

**Fig. 15** and **Fig. 16** show the impact of the cohesion strength on the net pressure and the fracture width. It can be found that the more plastic (lower cohesion strength) the formation is, the higher the net pressure is needed to initiate and propagate the fracture, furthermore, lower cohesion strength also leads to wider fracture geometry.

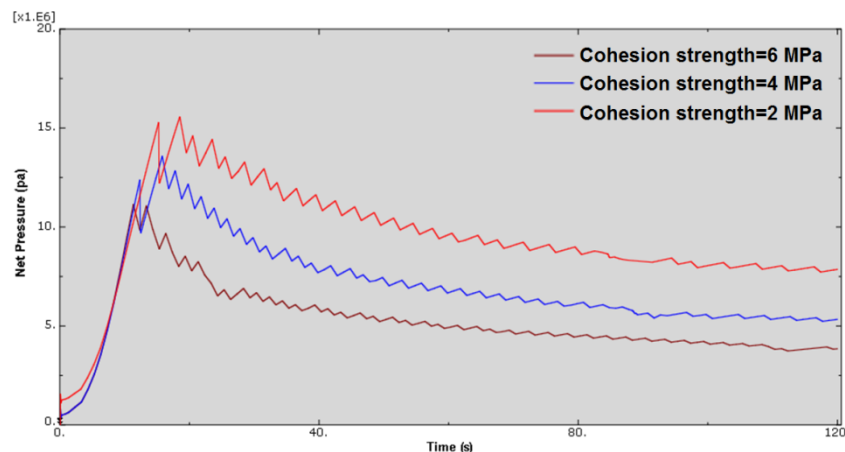


**Fig. 15**–Impact of cohesion strength on net pressure

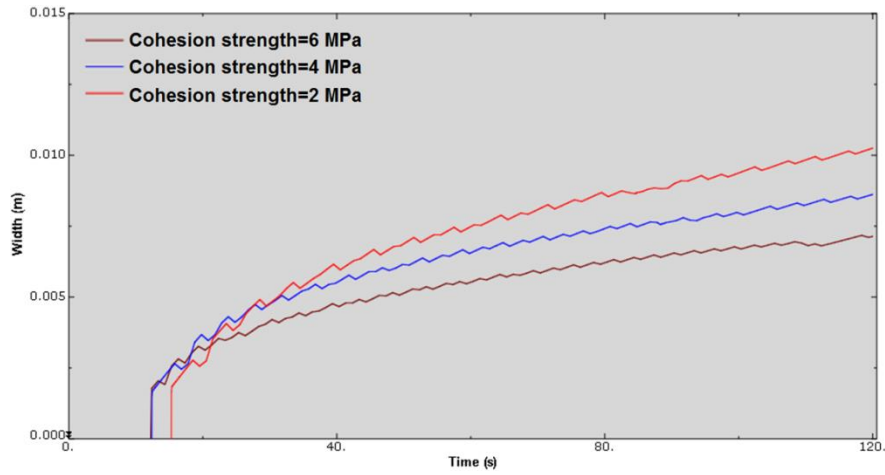


Fig. 16–Impact of cohesion strength on fracture width

Fig. 17 and Fig. 18 show the impact of the cohesion strength on plastic deformation and fracture geometry. The more plastic the formation is (with decreasing cohesion strength), the larger the area affected by plastic failures and the shorter the fracture length are. The area that affected by plastic deformation is within 0.4 m and 1 m (square mesh size is 0.2m around the pre-defined hydraulic fracture path) away from the fracture path for formations with 6 MPa and 4 MPa cohesion strength respectively, but it can extend to a few meters into the formation where the cohesion strength is only 2 MPa.

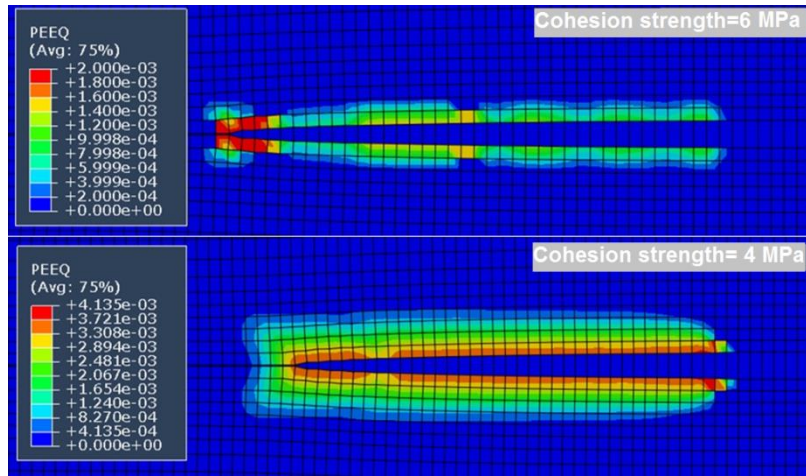


Fig. 17–Plastic strain and fracture geometry with 6MPa and 4MPa cohesion strength

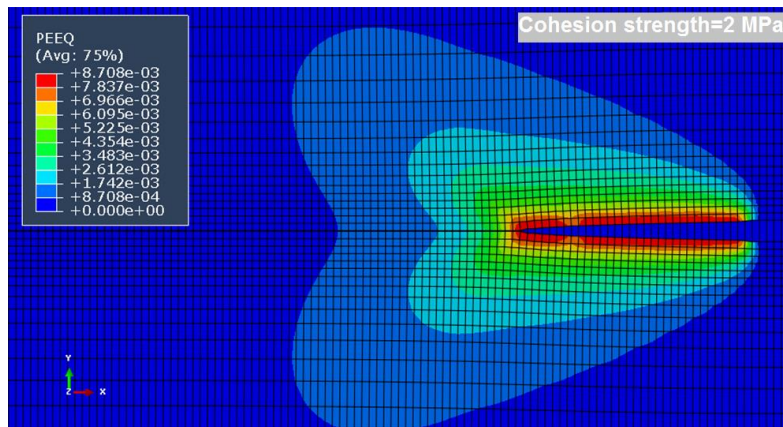


Fig. 18–Plastic strain and fracture geometry with 2MPa cohesion strength

**Conclusions and Discussions**

In this study, we first presented a brief literature review on hydraulic fracturing modeling based on the theory of Linear Elastic Fracture Mechanics and Cohesive Zone Method, and discussed the associated challenges when dealing with ductile rocks that

can undergo plastic deformations during hydraulic fracture propagation. Then, a novel poro-elasto-plastic model that combines Cohesive Zone Method and Mohr-Coulomb flow theory of plasticity was presented; this model is capable of modeling hydraulic fracture propagation in both brittle and ductile formations. More importantly, the impact of formation plastic properties on the fracturing process is deeply investigated and the results are compared with established poroelastic and modified poroelastic models. From the results of this research, we can conclude that:

1. The effects of formation plasticity on a hydraulic fracture are mostly controlled by in-situ stress contrast, cohesion strength of formation rock and pore pressure.
2. Ignoring plastic deformation when modeling hydraulic fracture propagation in formations that can undergo plastic deformations, such as poorly consolidated/unconsolidated sands or ductile shales, can lead to inaccurate prediction of fracture geometry, net pressure and fluid efficiency.
3. The method of using effective toughness (e.g., increases critical fracture energy in the cohesive zone) to account for formation plasticity can only partly mimic the consequences of increased toughness within the very close vicinity ahead of fracture tip, but it fails capturing the effect of plastic deformation that induced by shear failure within the whole affected area, so it may underestimate the fracture width and overestimate fracture length.
4. In comparison to brittle rock, ductile and highly deforming formations exhibit higher breakdown and propagation pressure. The more plastic the formation (lower cohesion strength), the higher is the net pressure required to initiate and propagate the fracture due to increased energy that absorbed by plastic deformations. Also lower cohesion strength lead to shorter and wider fracture geometry.
5. For effective modeling of hydraulic fracturing propagation in ductile formations, the effects of plastic deformation in the whole stimulated reservoir volume should be included. So using Cohesive Zone Method alone, which only accounts for in-elastic behavior at the fracture tip, is not adequate for modeling the overall effects of plastic damage within the entire affected region.

Even though the plastic behavior of poorly consolidated/unconsolidated sands and its impact on hydraulic fracturing has already attracted much attention in both academia and industry, the plasticity of clay rich, ductile shales has been largely overlooked in hydraulic fracturing design and execution, despite many laboratory and field studies have shown that shale rocks can exhibit plastic or even time dependent elastic-visco-plastic behavior. From the results of our study, it seems that the impact of formation plastic deformations on hydraulic fracturing is not trivial. If these ductile formations are treated as pure elastic, then our optimized hydraulic fracturing design may render suboptimal well performance, because of the unsound fracture geometry prediction and the corresponding unappropriated choice of proppant size and concentration. In some cases, the unexpected higher breakdown pressure needed in job execution may not be achievable at all, due to surface equipment and operational limitations.

For heterogeneous formations, the rock properties can transit between brittle and ductile along the section of a horizontal well and the formation themselves can as well be laminated with both brittle and ductile rock layers. A better understanding of the properties of ductile rocks and their impact on hydraulic fracture propagation and well performance is crucial to optimize hydraulic fracturing design in these formations. How these ductile rock intervals impact hydraulic fracture interactions (stress shadow effects), fracture height containment and interactions with natural fractures requires future investigations.

The poro-elasto-plastic hydraulic fracturing propagation model proposed in this study can be used as a powerful tool to address these issues and the results from our simulation study agree well with some field observations. Like for any other model, field data that combines reservoir characterization, fracture diagnostics and post-production analysis will be needed to calibrate this predictive model for a specific reservoir.

## Nomenclature

$A_L$	= Leakoff surface, $L^2$ , $m^2$
$c$	= Cohesion strength, $m/Lt^2$ , Pa
$C_L$	= Carter's leakoff coefficient, $L/\sqrt{t}$ , $m/\sqrt{s}$
$d$	= Initial thickness of cohesive surfaces, L, m
$E$	= Young's modulus, $m/Lt^2$ , Pa
$G$	= Potential function
$G_I^c$	= Fracture critical energy in Mode I, $mL^2/t^2$ , J
$G_{II}^c$	= Fracture critical energy in Mode II, $mL^2/t^2$ , J
$G_{III}^c$	= Fracture critical energy in Mode III, $mL^2/t^2$ , J
$\mathbf{k}$	= Formation permeability tensor in formation, $L^2$ , md
$K_n$	= Cohesive stiffness, $m/L^2t^2$ , Pa/m
$p$	= Pore pressure, $m/Lt^2$ , Pa
$q_f$	= Flow rate along fracture per unit height, $L^2/t$ , $m^3/(s \cdot m)$



$q_l$	= Leakoff rate per unit fracture surface area, $L^2/t, m^3/(s \cdot m^2)$
$q_m$	= Fluid flux velocity in formation matrix, L/t, m/s
$S_p$	= Spurt loss, L, m
$t$	= Surface traction on cohesive interface, m/Lt <sup>2</sup> , Pa
$T$	= Traction force, m/Lt <sup>2</sup> , Pa
$T_{Max}$	= Cohesive tensile strength, m/Lt <sup>2</sup> , Pa
$V_L$	= Cumulative leakoff volume, $L^3, m^3$
$w$	= Fracture width, L, m
$\delta$	= Displacement, L, m
$\delta_0$	= Displacement at damage initiation, L, m
$\delta_f$	= Displacement at failure, L, m
$\delta_m$	= Effective displacement, L, m
$\varepsilon$	= Normal strain
$K_{IC}$	= Rock fracture toughness in Mode I, $m/\sqrt{Lt^2}, Pa\sqrt{m}$
$\mu$	= Fluid viscosity, m/Lt, cp
$\nu$	= Poisson's ratio
$v_L$	= Leakoff rate, L/t, m/s
$V_L$	= Cumulative leak-off volume, $L^3, m^3$
$\sigma$	= Stress, m/Lt <sup>2</sup> , Pa
$\tau_f$	= Shear strength, m/Lt <sup>2</sup> , Pa
$\varphi$	= Friction angle

## References

- Adachi, J. and Detournay, E. 2008. Plain strain propagation of a hydraulic fracture in permeable rock. *Engineering Fracture Mechanics*, **75**(16), 4666 – 4694. <http://dx.doi.org/10.1016/j.engfracmech.2008.04.006>.
- Afrouz, A. 1992. *Practical Handbook of Rock Mass Classification Systems and Modes of Ground Failure*. First Edition. Boca Raton, Florida: CRC Press.
- Barenblatt, G.I. 1959. The formation of equilibrium cracks during brittle fracture: general ideas and hypothesis, axially symmetric cracks. *Journal of Applied Mathematics and Mechanics*, **23**:622–636. [http://dx.doi.org/10.1016/0021-8928\(59\)90157-1](http://dx.doi.org/10.1016/0021-8928(59)90157-1).
- Barenblatt, G.I. 1962. The mathematical theory of equilibrium cracks in brittle fracture. *Advanced in Applied Mechanics*. Academic Press, New York, pp. 55-129.
- Benzeggagh, M.L., and Kenane, M. 1996. Measurement of mixed-mode delamination fracture toughness of unidirectional glass/epoxy composites with mixed-mode bending apparatus. *Composites Science and Technology* **56**:439–449. [http://dx.doi.org/10.1016/0266-3538\(96\)00005-X](http://dx.doi.org/10.1016/0266-3538(96)00005-X).
- Biot, M. A. 1941. General theory of three dimensional consolidation. *Journal of Applied Physics*, **12**(2), 155–164. <http://dx.doi.org/10.1063/1.1712886>.
- Boone, T.J., and Ingraffea, A.R. 1990. A numerical procedure for simulation of hydraulically driven fracture propagation in poroelastic media. *International Journal for Numerical and Analytical Methods in Geomechanics*, **14**:27–47. <http://dx.doi.org/10.1002/nag.1610140103>.
- Carrier, B. and Granet, S. 2013. Finite Element Modeling of Fluid-Driven Fracture in Permeable Medium. *Poromechanics (V)*:462-470. <http://dx.doi.org/10.1061/9780784412992.055>.
- Chen, Z.R., Bungler, A.P., Zhang, et al. 2009. Cohesive zone finite element based modeling of hydraulic fractures. *Acta Mechanica Solida Sinica*, **22**(5):443–452. [http://dx.doi.org/10.1016/S0894-9166\(09\)60295-0](http://dx.doi.org/10.1016/S0894-9166(09)60295-0).
- Dean, R.H., and Schmidt, J.H. 2009. Hydraulic fracture predictions with a fully coupled geomechanical reservoir simulator. *SPE Journal*. **14**(4):707–714. SPE-116470-PA. <http://dx.doi.org/10.2118/116470-PA>.
- Detournay, E. and Garagash, D. I. 2003. The near-tip region of a fluid-driven fracture propagating in a permeable elastic solid. *Journal of Fluid Mechanics*, **494**, 1–32. <http://dx.doi.org/10.1017/S0022112003005275>.
- Dugdale, D.S. 1960. Yielding of steel sheets containing slits. *Journal of the Mechanics and Physics of Solids*, **8**:100–104. [http://dx.doi.org/10.1016/0022-5096\(60\)90013-2](http://dx.doi.org/10.1016/0022-5096(60)90013-2).
- E. Orowan. 1955. Energy criteria of fracture. *Weld. Res. Supp.*, **34**:157–160

- Economides, M. and Nolte, K. 2000. *Reservoir Stimulation*, 3rd edition. Chichester, UK: John Wiley & Sons.
- Geertsma, J. and De Klerk, F. 1969. A rapid method of predicting width and extent of hydraulic induced fractures. *Journal of Petroleum Technology*, 246:1571–1581. SPE-2458-PA. <http://dx.doi.org/10.2118/2458-PA>.
- Germanovich, L.N., Astakhov, D. K., Shlyapobersky, J. et al. 1998. Modeling multi-segmented hydraulic fracture in two extreme cases: No leak-off and dominating leak-off. *International Journal of Rock Mechanics and Mining Sciences*, **35**(4-5), 551- 554. [http://dx.doi.org/10.1016/S0148-9062\(98\)00119-3](http://dx.doi.org/10.1016/S0148-9062(98)00119-3).
- Griffith, A.A. 1921. The phenomena of rupture and flow in solids. *Philosophical Transactions of the Royal Society*, 221:163–198. <http://dx.doi.org/10.1098/rsta.1921.0006>.
- Howard, G.C., and Fast, C.R. 1970. *Hydraulic Fracturing Monograph. SPE Monograph*, Vol. 2. Henry L. Doherty Series. New York: Society of Petroleum Engineers.
- Irwin G.R. 1957. Analysis of stresses and strain near the end of crack traversing a plate. *J. Appl. Mech.*, T. ASME, 24, 361-364.
- Kanninen, M.F., and Popelar, C.H. 1985. *Advanced fracture mechanics*, first edition. Oxford, UK: Oxford University Press.
- Khristianovich, S., and Zheltov, Y. 1955. Formation of vertical fractures by means of highly viscous fluids. *Proc. 4th World Petroleum Congress*, Rome, Sec. II, 579–586.
- Marongiu-Porcu, M., Ehlig-Economides, C.A., Retnanto, A., and Economides, M.J. 2014. Comprehensive Fracture Calibration Test Design. Paper SPE 168634 presented at the SPE Hydraulic Fracturing Technology Conference, held in Woodlands, Texas, USA, 4-6 February. <http://dx.doi.org/10.2118/168634-MS>.
- Mokryakov, V. 2011. Analytical solution for propagation of hydraulic fracture with Barenblatt's cohesive tip zone. *International Journal of Fracture*, 169:159–168. <http://dx.doi.org/10.1007/s10704-011-9591-0>.
- Nassir, M. 2013. Geomechanical Coupled Modeling of Shear Fracturing in Non-Conventional Reservoir. PHD dissertation, University of Calgary, Alberta, Canada.
- Nordgren, R. 1972. Propagation of vertical hydraulic fractures. *Journal of Petroleum Technology*, 253:306–314. SPE-3009-PA . <http://dx.doi.org/10.2118/3009-PA>.
- Notle, K.G. 1986. A General Analysis of Fracturing Pressure Decline With Application to Three Models. *SPE Formation Evaluation*, 1(06): 571-583. <http://dx.doi.org/10.2118/12941-PA>
- Papanastasiou, P. 1997. The influence of plasticity in hydraulic fracturing. *International Journal of Fracture*, **84**(1), 61–79. <http://dx.doi.org/10.1023/A:1007336003057>.
- Papanastasiou, P. 1999. The effective fracture toughness in hydraulic fracturing. *International Journal of Fracture*, **96**(2), 127–147. <http://dx.doi.org/10.1023/A:1018676212444>.
- Parker, M., Petre, E., Dreher, D., and Buller, D. 2009. Haynesville Shale: Hydraulic Fracture Stimulation Approach. Paper 0913 presented at the International Coalbed & Shale Gas Symposium, Tuscaloosa, Alabama, USA, 18–22 May.
- Perkins, T. and Kern, L. 1961. Widths of hydraulic fractures. *Journal of Petroleum Technology*, Trans. AIME, 222:937–949. <http://dx.doi.org/10.2118/89-PA>.
- Sarris, E., and Papanastasiou, P. 2012. Modeling of Hydraulic Fracturing in a Poroelastic Cohesive Formation. *International Journal of Geomechanics*, **12**(2), 160–167. [http://dx.doi.org/10.1061/\(ASCE\)GM.1943-5622.0000121](http://dx.doi.org/10.1061/(ASCE)GM.1943-5622.0000121).
- Sone, H., and Zoback, M.D. 2011. Visco-plastic Properties of Shale Gas Reservoir Rocks. Presented at the 45th U.S. Rock Mechanics / Geomechanics Symposium, June 26 - 29, San Francisco, California. ARMA-11-417
- Stegent, N., Wagner, A., Mullen, J. and Borstmayer, R. 2010. Engineering a Successful Fracture-Stimulation Treatment in the Eagle Ford Shale. Paper SPE 136183 presented at the SPE Tight Gas Completions Conference, San Antonio, Texas, USA 2-3 November. <http://dx.doi.org/10.2118/136183-MS>
- Tomar, V., Zhai, J., and Zhou, M. 2004. Bounds for element size in a variable stiffness cohesive finite element model. *International Journal for Numerical Methods in Engineering*, **61**(11): 1894-1920. <http://dx.doi.org/10.1002/nme.1138>.
- Turon, A., Camanho, P.P., Costa, J. et al. 2006. A damage model for the simulation of delamination in advanced composites under variable-model loading. *Mechanics of Materials*, **38** (11): 1072–1089. <http://dx.doi.org/10.1016/j.mechmat.2005.10.003>.
- Valkó, P.P., and Economides, M.J. 1999. Fluid-Leakoff Delineation in High-Permeability Fracturing. *SPE Production & Facilities*, **14** (2):17–130. SPE-37403-MS. <http://dx.doi.org/10.2118/56135-PA> .
- Van Dam, D.B., Papanastasiou, P., and De Pater, C.J. 2002. Impact of rock plasticity on hydraulic fracture propagation and

- closure. *SPE Production & Facilities*, **17**(3):149–159. SPE-63172-MS. <http://dx.doi.org/10.2118/63172-MS>.
- Vermeer, P. A., and De Borst, R. 1984. Non-Associated Plasticity for Soils, Concrete and Rock. *Heron* **29**(3): 3-64.
- Wang, H. 2015a. Numerical Modeling of Non-Planar Hydraulic Fracture Propagation in Brittle and Ductile Rocks using XFEM with Cohesive Zone Method. To be published in *Journal of Petroleum Science and Engineering*
- Wang, H. 2015b. Poro-Elasto-Plastic Modeling of Complex Hydraulic Fracture Propagation: Simultaneous Multi-Fracturing and Producing Well Interference. To be published in *Acta Mechanica*.
- Weng, X. 2014. Modeling of Complex Hydraulic Fractures in Naturally Fractured Formation. *Journal of Unconventional Oil and Gas Resources*, Vol. 9, pp. 114-135. <http://dx.doi.org/10.1016/j.juogr.2014.07.001>
- Yao, Y. 2012. Linear Elastic and Cohesive Fracture Analysis to Model Hydraulic Fracture in Brittle and Ductile Rocks. *Rock Mechanics and Rock Engineering*, 45:375–387. <http://dx.doi.org/10.1007/s00603-011-0211-0>.
- Yuan, R., Jin, L., Zhu, C., Vitthal, S., and Xu, B. 2013. High Pressure Stimulation - Impact of Hydraulic Fracture Geometry to Unconventional Gas Appraisal and Development in Compressional Settings. Paper SPE 166348 presented at the SPE Annual Technical Conference and Exhibition, held in New Orleans, Louisiana, USA, 30 September-2 October. <http://dx.doi.org/10.2118/166348-MS>